QUASI-SIMULTANEOUS VISCOUS-INVISCID INTERACTION FOR THREE-DIMENSIONAL TURBULENT WING FLOW

E.G.M. Coenen, A.E.P. Veldman and G. Patrianakos
EGMC & AEPV: Department of Mathematics, University of Groningen, The Netherlands
GP: Department of Aerospace Engineering, University of Bristol, United Kingdom

Keywords: *Viscous-inviscid interaction, three-dimensional boundary layer, swept wings, quasi-simultaneous coupling technique, panel method*

Abstract

A fully three-dimensional viscous-inviscid interaction method is developed for the calculation of steady incompressible flow over transport wing configurations. The external inviscid flow is computed with a constant-potential (Dirichlet) panel method and the viscous layer is described with three turbulent integral boundary layer equations, in a Cartesian coordinate system. The interaction between the two regions is modelled via the wall transpiration velocity concept. From the used external flow formulation approximations for the edge velocity components are derived, required for the quasi-simultaneous coupling. The boundary layer equations are discretised with a finite volume scheme, and solved simultaneously with the approximations for the external flow by Newton's method. Results are presented for unswept and swept wing cases and are compared with experiment and other computational results.

1 Introduction

Over the past years a lot of progress has been made with Navier-Stokes simulation for the computation of airflow around realistic wing configurations. However, even with today's computers, the computational cost involved renders this approach impractical within a design-optimisation environment.

The alternative is to use interactive boundary layer theory which involves special techniques to couple the viscous and inviscid regions to find the whole flow solution. For two-dimensional flow problems extensive research has been done into viscous-inviscid interaction (VII) and it has shown to be very successful [16]. The VII methods proved to be very efficient and they produced accurate answers to practical problems and this at much lower computational cost than Navier-Stokes solvers.

Despite this success in two dimensions, the extension to fully three-dimensional viscous-inviscid interaction has scarcely been attempted. However, expecting similar advantages in three dimensions, research at Bristol and Groningen was undertaken to come to the development of a fully three-dimensional VII method.

The three-dimensional boundary layer equations are taken in integral form, reducing the computational effort and immediately providing information about the boundary layer quantities with little loss in accuracy. A set-back however, is the great dependency of empiricism by the integral methods and certain information is not yet available for three-dimensional flows.

Unlike the steady two-dimensional problem, where the integral boundary layer is simply described by a set of ordinary differential equations, the three-dimensional boundary layer equations are quite complex. The three-dimensional steady problem corresponds with the two-dimensional unsteady problem and the boundary layer is given by three non-linear partial differential equations

[6]. The system of equations, with the velocity distribution prescribed, is fully hyperbolic, having three real and distinct characteristics [20], [7].

Direct coupling techniques have been investigated for the calculation of three-dimensional interacted flows [7], [22], [10]. It was found that as in two dimensions the direct scheme breaks down due to the development of a non-physical singularity. For two-dimensional flow this is related to the vanishing skin-friction, leading to a (Goldstein) singularity. In three dimensions the zero-skin-friction-point will generally not lead to a singularity, but under certain conditions the characteristic lines tend to converge, similar to shock formation, which can lead to a singularity.

In two dimensions it was shown that the singularity at separation can be avoided if the boundary layer is solved in inverse mode with a prescribed wall transpiration velocity instead of a prescribed external velocity distribution. The same is true in three dimensions. The inverse technique removes the non-physical singularity that can occur from the focusing of a characteristic line [7], [10].

Following Stewartson's theory, for flow calculations with regions with strong interaction, the boundary layer should not be considered separately from the external inviscid flow as in the previously described direct and inverse methods. Le Balleur [15] takes this into account by combining the two regions via a matching condition in his semi-inverse method for three-dimensional flows. However, the use of an update procedure can be avoided by simultaneously solving the external and viscous regions, which has shown in two dimensions to be the most robust approach for separated flows [16]. Fully simultaneous algorithms have been presented by Drela *et al.* for two- and three-dimensional flow [8], [21]. A simpler alternative is to use the quasi-simultaneous method, developed by Veldman [24], which is applied here.

Instead of solving the boundary layer and the outer flow completely simultaneously, the quasi-simultaneous method solves the boundary layer together with suitable approximations for the outer flow. The inviscid calculations are performed with a prescribed wall transpiration velocity, as before with the direct method.

The quasi-simultaneous method has a straightforward extension to three dimensions and was shown to work successfully by Edwards [9] for the calculation of three-dimensional laminar flow over a flat plate with protuberance and by Van der Wees *et al.* [23] for the computation of transonic flow over wing/body configurations.

The integral boundary layer equations are determined in a Cartesian coordinate system and discretised via an upwind finite volume scheme. In this way, the calculation of cumbersome metric gradients, which have to be evaluated for the traditional boundary layer formulation in a general curvilinear coordinate system, is avoided.

For the computation of the external inviscid flow a constant potential Dirichlet panel method is used. The panel method is only valid for irrotational subsonic flow but has the advantage to be less expensive than an Euler or full potential method. The latter methods however, can be easily implemented in the present quasi-simultaneous calculation scheme.

The developed program is tested for two wing flow cases and results are compared with experiment and other computational results.

2 Boundary layer region

The boundary layer is described by three turbulent integral boundary layer equations transformed to a local Cartesian coordinate system (x,y,z). The x and y directions lie in the plane tangent to the surface of the boundary layer and the z direction is normal to the plane, as shown in figure 1. The set of three-dimensional integral boundary layer equations is:

$$\frac{\partial}{\partial x}(\theta_{xx}q_e^2)+\frac{\partial}{\partial y}(\theta_{xy}q_e^2) = -q_e\delta_x^*\frac{\partial u_{e_x}}{\partial x}-q_e\delta_y^*\frac{\partial u_{e_x}}{\partial y}+\tau_{w_x}, \tag{1}$$

$$\frac{\partial}{\partial x}(\theta_{yx}q_e^2)+\frac{\partial}{\partial y}(\theta_{yy}q_e^2) = -q_e\delta_x^*\frac{\partial u_{e_y}}{\partial x}-q_e\delta_y^*\frac{\partial u_{e_y}}{\partial y}+\tau_{w_y}, \tag{2}$$

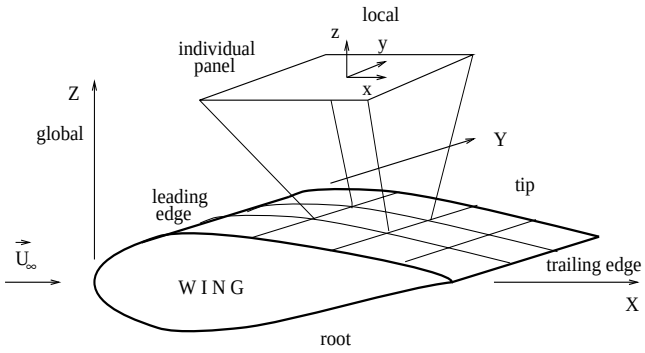

Fig. 1 Global (X,Y,Z) and local (x,y,z) Cartesian coordinate systems.

$$\frac{1}{q_e}\frac{\partial}{\partial x}(u_{e_x}\delta - q_e\delta_x^*) + \frac{1}{q_e}\frac{\partial}{\partial y}(u_{e_y}\delta - q_e\delta_y^*) = C_E. \qquad (3)$$

Equations (1) and (2) are the x- and y-integral momentum equations and equation (3) is the entrainment equation. The two momentum equations in a Cartesian system are derived in [19]. The entrainment equation can be found, as was shown in two dimensions by Head, by integrating the continuity equation across the boundary layer [3]. The entrainment coefficient C_E describes the (non-dimensional) rate at which fluid from the external inviscid flow enters through the external edge of the boundary layer. The above equations are hyperbolic and have three real and distinct characteristic directions. The characteristics correspond to the tangent of the angle they make with the x-direction and are bounded by the

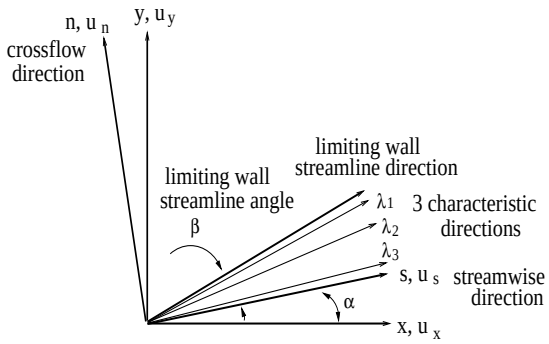

Fig. 2 Cartesian and streamline coordinate systems and characteristic directions.

direction of the external streamline and the limiting wall streamline, see figure 2. One characteristic almost corresponds with the limiting wall streamline as was described in [7].

The three boundary layer equations require three independent boundary layer variables. All the other boundary layer quantities should be determined from these three variables using closure relations. In order to make use of the established closure relations, based on streamwise and crossflow velocity profiles, it is necessary to work in a streamline coordinate system. The boundary layer quantities in the x,y system need to be transformed to the streamline s,n system. Looking again at figure 2, it is seen that via vector rotation the x,y quantities can be expressed in s,n quantities. The relationship between the two systems is easily given in terms of the velocities:

$$\begin{aligned} u_x &= u_s\cos\alpha - u_n\sin\alpha, \\ u_y &= u_s\sin\alpha + u_n\cos\alpha, \end{aligned}$$

where α is the angle between the x and s directions. With the above relationship the streamwise and crossflow integral thicknesses can be easily determined.

For streamwise closure the correlations described in the papers by Ashill *et al.* [1], Green [11] and Houwink and Veldman [12] are to be used, the latter giving a suitable H-H_1 relation for separated flow. For C_E an empirical expression in three dimensions is not yet available and it is assumed that the empirical relationship for C_E in two dimensions holds [22].

The unknowns in the crossflow direction are determined by Mager's crossflow velocity profile, in which it is assumed that the flow direction varies monotonically across the boundary layer. Unlike Johnston's crossflow profile, Mager allows for zero friction and can be used in the wake. With Mager's profile and a streamwise power law profile to determine a relationship between H and H_1, the boundary layer thicknesses become expressions in terms of only θ_{ss}, H and β, where β is the limiting wall streamline angle. A set-back of using Mager's crossflow velocity profile is that it has been established only for fairly small values of β. For β close to 45^o it gives implausible

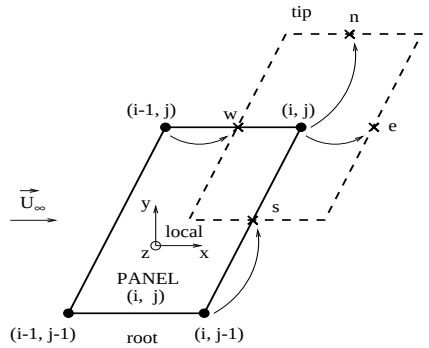

Fig. 3 Parallelogram panel (i,j).

values for the integral thicknesses [16]. It would therefore be more accurate to use the more sophisticated Cross velocity profile which is hoped soon to include in the present calculation method.

For the discretisation of the equations, a grid has been constructed from parallelograms, as shown in figure 3. As discussed before, every parallelogram panel has its own local Cartesian coordinate system, with the origin in its centre. The parallelogram panel (i,j) is then defined by the four edge points (x_{i-1j-1},y_{i-1j-1}), (x_{ij-1},y_{ij-1}), (x_{ij},y_{ij}), (x_{i-1j},y_{i-1j}). The grid being non-orthogonal, the equations are discretised with a finite volume method. Around grid point (x_{ij},y_{ij}) a cell is chosen of which (x_{ij},y_{ij}) is the centre. The new cell, drawn with the dashed lines in figure 3, has points n(orth), e(ast), s(outh) and w(est) lying halfway the cell edges. Furthermore, point s lies halfway gridpoints (x_{ij-1},y_{ij-1}) and (x_{ij},y_{ij}) and point w lies halfway gridpoints (x_{i-1j},y_{i-1j}) to (x_{ij},y_{ij}) of panel (i,j). In order to obtain a stable system, upwinding is applied by transporting the values at (i,j) to the points n and e and the values at $(i,j-1)$, respectively $(i-1,j)$, to point s, respectively w. The corresponding discretisation of the x-momentum equation (1) in point (x_{ij},y_{ij}) becomes:

$$\frac{\theta_{xx_{ij}}q^2_{e_{ij}}-\theta_{xx_{i-1j}}q^2_{e_{i-1j}}}{x_{ij}-x_{i-1j}}+\frac{\theta_{xy_{ij}}q^2_{e_{ij}}-\theta_{xy_{ij-1}}q^2_{e_{ij-1}}}{y_{ij}-y_{ij-1}}-$$
$$\frac{\theta_{xy_{ij}}q^2_{e_{ij}}-\theta_{xy_{i-1j}}q^2_{e_{i-1j}}}{y_{ij}-y_{ij-1}}\,\frac{x_{ij}-x_{ij-1}}{x_{ij}-x_{i-1j}}+$$
$$q_{e_{ij}}\delta^*_{x_{ij}}\frac{u_{e_{x_{ij}}}-u_{e_{x_{i-1j}}}}{x_{ij}-x_{i-1j}}+q_{e_{ij}}\delta^*_{y_{ij}}\left(\frac{u_{e_{x_{ij}}}-u_{e_{x_{ij-1}}}}{y_{ij}-y_{ij-1}}-\right.$$
$$\left.\frac{u_{e_{x_{ij}}}-u_{e_{x_{i-1j}}}}{y_{ij}-y_{ij-1}}\,\frac{x_{ij}-x_{ij-1}}{x_{ij}-x_{i-1j}}\right)\;=\;\tau_{w_{x_{ij}}}.$$

Similar expressions exist for the other boundary layer equations.

Taking the flow of information into account, the above discretisation is only valid if the characteristics going through (i,j) cross the cell edge (x_{i-1j-1},y_{i-1j-1}) to (x_{i-1j},y_{i-1j}) or the cell edge (x_{i-1j-1},y_{i-1j-1}) to (x_{ij-1},y_{ij-1}). This is the case, unless the angle $\beta+\alpha$, which corresponds with the angle the most outbound characteristic λ_1 makes with the x-direction in figure 2, is smaller than zero or greater than $90^o-\Lambda$, where Λ is the sweep angle. For the case that $\beta+\alpha<0$, there is no problem. The discretisation at point (i,j) should however be done with panel $(i,j+1)$ instead. However, for the case that $\beta+\alpha>90^o-\Lambda$, the flow is parallel to the leading edge which corresponds to separation. A scheme dealing with characteristics coming from upstream is being implemented at present. Artificial diffusion is to be added, similar to the Jameson's approach for Euler calculations, to obtain a discretisation capable of dealing with the turning of the characteristic directions [13].

3 Inviscid flow region

In the external inviscid region the flow is assumed to be incompressible and irrotational. The inviscid flow field over the wing can then be modelled with three-dimensional potential theory [18]. Along the wing surface a source sheet of strength σ is distributed together with a doublet sheet of strength μ. The latter is also extended into the wake. The total potential Φ is written:

$$\Phi\;=\;\Phi_\infty-\int_{S_B}\frac{\sigma}{4\pi r}\mathrm{d}S+\int_{S_W+S_B}\mu\frac{\partial}{\partial n}\frac{1}{4\pi r}\mathrm{d}S. \qquad (4)$$

A transpiration velocity boundary condition provides the coupling mechanism between the inviscid and viscous regions. The boundary condition is implemented by applying an extra viscous

source distribution in the invisicid model to simulate the displacement effect of the boundary layer. The viscous source strength, σ_{vis}, is given by:

$$\sigma_{vis} = \frac{\partial}{\partial x}(q_e \delta_x^*) + \frac{\partial}{\partial y}(q_e \delta_y^*). \quad (5)$$

On the wing surface, instead of using a Neumann boundary condition of prescribed normal velocity at the surface, a Dirichlet boundary condition is applied. The total potential inside the body, Φ_i, is specified to be $\Phi_i = \Phi_\infty$ on the boundary. With this and (5), equation (4) for collocation points inside the body thus becomes:

$$\int_{S_B+S_W} \mu \frac{\partial}{\partial n}\frac{1}{4\pi r}\,\mathrm{d}S = \int_{S_B} \frac{\sigma_{inv}}{4\pi r}\,\mathrm{d}S + \int_{S_B+S_W} \frac{\sigma_{vis}}{4\pi r}\,\mathrm{d}S. \quad (6)$$

The inviscid source strength σ_{inv} can be found from the freestream, and the viscous source strength σ_{vis} is to be given by the boundary layer equations. To determine the problem uniquely, an implicit Kutta condition is used to define the doublet strength in the wake. A set of algebraic equations remains to be solved for the unknown doublet strengths on the surface of the wing.

For the discretisation of the above system the wing body and wake are divided into surface panel elements as was shown in figure 1. Furthermore, the source and doublet strengths are assumed to be constant over a panel. Relations for the unknown doublet strengths can therefore be determined from equation (6) in the midpoint of each panel. However, as relations for the edge velocity components are required for the viscous-inviscid interaction method some further manipulations are performed, using that the doublicity gradients determine the global velocity vector in the end points of the panels [14]. Finally, the above leads to the equations for the global edge velocity components of the following form:

$$u_{e_{X_{ij}}} = u_{0_{X_{ij}}} + \sum q_{e_{kl}} \left[A_{X_{ijkl}} \delta^*_{x_{kl}} + B_{X_{ijkl}} \delta^*_{y_{kl}} \right], \quad (7)$$

$$u_{e_{Y_{ij}}} = u_{0_{Y_{ij}}} + \sum q_{e_{kl}} \left[A_{Y_{ijkl}} \delta^*_{x_{kl}} + B_{Y_{ijkl}} \delta^*_{y_{kl}} \right], \quad (8)$$

$$u_{e_{Z_{ij}}} = u_{0_{Z_{ij}}} + \sum q_{e_{kl}} \left[A_{Z_{ijkl}} \delta^*_{x_{kl}} + B_{Z_{ijkl}} \delta^*_{y_{kl}} \right], \quad (9)$$

where the summation is over $k = 1$ to N and $l = 1$ to M, with N the number of segments into which the contour of the wing section is divided and M the number of spanwise segments. The velocity components u_{0_X}, u_{0_Y} and u_{0_Z} represent the global undisturbed inviscid velocity and matrices A and B contain the discretisation of the geometry and the differentiation of the viscous source (5).

On a flat square grid, the matrix entries of A_X correspond with the matrix entries of B_Y and similar do the matrix entries of A_Y correspond with the matrix entries of B_X. Furthermore, matrices A_X and B_Y can be shown to be diagonally dominant and to have positive values on the main diagonal and negative values on the off-diagonals. These matrix properties will have a positive influence on the iteration process.

In the wake, which is split into an upper and lower wake, similar relations as (7), (8) and (9) are determined for the interaction with the boundary layer, using $\overrightarrow{U_{e_{ij}}} = \nabla \Phi_{ij}$.

4 Quasi-simultaneous coupling

The interaction technique applied to couple the set of boundary layer equations (1), (2) and (3) to the inviscid flow equations (7), (8) and (9) is the quasi-simultaneous method [24].

In two dimensions the quasi-simultaneous method was shown to be the most efficient and robust of the various coupling algorithms [16]. Especially when calculating regions with strong interaction the external inviscid flow and boundary layer should be treated simultaneously, rather than iteratively.

A requirement of the quasi-simultaneous method is to find suitable approximations for the external flow equations, which are to be solved together with the boundary layer equations. These approximations are termed interaction laws and describe the interaction with the boundary layer. The interaction laws are employed in a deficit formula and thus will not influence the final solution. Convergence speed however, depends on how accurately the approximations have been chosen.

Three interaction laws for the global velocity

components have been derived from the external flow formulation described. The simple approximations for $u_{e_{X_{ij}}}$, $u_{e_{Y_{ij}}}$ and $u_{e_{Z_{ij}}}$ are taken to be:

$$u_{e_{X_{ij}}} \approx u_{0_{X_{ij}}} + \sum_{k=i-1}^{i+1} \tilde{A}_{X_{ijkj}} q_{e_{kj}} \delta^*_{x_{kj}}, \quad (10)$$

$$u_{e_{Y_{ij}}} \approx u_{0_{Y_{ij}}} + \sum_{l=j-1}^{j+1} \tilde{B}_{Y_{ijil}} q_{e_{il}} \delta^*_{y_{il}}, \quad (11)$$

$$u_{e_{Z_{ij}}} \approx u_{0_{Z_{ij}}}. \quad (12)$$

The approximations for u_{e_X} and u_{e_Y}, contain boundary layer information terms, which for u_{e_Z} are not included. Tridiagonal matrices $\tilde{A}_X$ and $\tilde{B}_Y$ are constructed in the same way as matrices A_X and B_Y, however, only the influence of the four neighbouring panels, which is most important for node point (i,j), is included. In equations (10) and (11) the summation is done from $k = i-1$ to $i+1$, respectively $l = j-1$ to $j+1$.

For simplification, u_{e_X} only has the contribution from the $q_e\delta^*_x$ part, as the influence of the $q_e\delta^*_y$ part is less important. Velocity u_{e_Y} has its main contribution from $q_e\delta^*_y$. For u_{e_Z} the $q_e\delta^*_x$ and $q_e\delta^*_y$ contributions are very small, the local z-direction being normal to the panels, and have therefore both been omitted. The matrix entries for $\tilde{A}_X$, respectively $\tilde{B}_Y$, have as before in (7) and (8) the correct sign at the main diagonal and a regular behaviour, which will prove favourably towards convergence speed.

If the operators E, for the external flow calculation, and I, for the interaction law calculation, are introduced, then the interaction law equations in defect formulation, which are solved together with the boundary layer equations, can be written symbolically as follows:

$$u_{e_X}^{(n+1)} - I_X[\delta_x^{*(n+1)}, \delta_y^{*(n+1)}] = E_X[\delta_x^{*(n)}, \delta_y^{*(n)}] - I_X[\delta_x^{*(n)}, \delta_y^{*(n)}], \quad (13)$$

$$u_{e_Y}^{(n+1)} - I_Y[\delta_x^{*(n+1)}, \delta_y^{*(n+1)}] = E_Y[\delta_x^{*(n)}, \delta_y^{*(n)}] - I_Y[\delta_x^{*(n)}, \delta_y^{*(n)}], \quad (14)$$

$$u_{e_Z}^{(n+1)} - I_Z[\delta_x^{*(n+1)}, \delta_y^{*(n+1)}] = E_Z[\delta_x^{*(n)}, \delta_y^{*(n)}] - I_Z[\delta_x^{*(n)}, \delta_y^{*(n)}]. \quad (15)$$

The right-hand-sight is known and the above three equations together with the three boundary layer equations will produce three new velocities and three new boundary layer values. From the calculated three boundary layer values new viscous source strengths σ_{vis} are determined for a new external inviscid flow calculation.

The boundary layer calculations are repeated three times before a new inviscid calculation is started which is done in order to make full use of the downstream information present in the interaction laws. Relaxation can be applied to the interaction laws for the more severe flow cases to improve convergence.

5 Solution method

The constructed discrete equations, consisting of the boundary layer equations and the interaction laws, are solved simultaneously along a column of points. Going from root to tip, each point is treated individually with a pointwise Newton scheme until convergence for the whole column is reached. The solution is then marched downstream along the X-direction, which corresponds approximately with the external flow direction.

The unknowns vector $\vec{U}$ to be solved for each pointwise Newton iteration is:

$$\vec{U} = (\theta_{ss}, H, \beta, u_{e_X}, u_{e_Y}, u_{e_Z})^t,$$

which is defined in the node points of the panels. The three boundary layer variables are taken in the streamline coordinate system, whereas the three velocity components are taken in the global Cartesian system.

No coupling takes place at the image plane and wing tip and boundary conditions are applied. The flow along the root should be parallel to the image plane, which leads to a symmetry condition assuming a zero gradient in the direction normal to the plane. Near the tip outflow is assumed, leading to a Neumann boundary condition of zero-spanwise gradient.

Initial conditions are required for the unknowns vector $\vec{U}$. For this, either a previously calculated nearby solution is used or the solution for two-dimensional turbulent flow over a flat plate is prescribed.

The solution at the trailing edge is calculated via extrapolation, as no interaction law matrices have been determined there.

The laminar part of the flow, till (tripped) transition, is calculated with a two-dimensional Thwaites method, using direct coupling.

6 Results and discussion

The above described three-dimensional viscous-inviscid interaction method has been applied to several test cases and some results are presented in this section. Initial results of the method for (quasi-)three-dimensional flow can be found in an earlier paper by the same authors [5].

The first calculation was performed to simulate quasi-two-dimensional flow over an unswept symmetric wing of high aspect ratio. For verification the computed results are compared with a two-dimensional VII program which has been constructed following a similar approach as the present method [4]. The second calculation was performed for a 45^o swept wing to demonstrate the three-dimensional capabilities of the method.

6.1 Quasi-two-dimensional wing flow

For the simulation of quasi-two-dimensional flow an unswept NACA0012 wing configuration is used with an aspect ratio of 14. The freestream Reynolds number was taken 9×10^6 and results have been obtained at an incidence $\alpha = 4^o$. Mid-wing the flow has the least influence of the tip and root effects, and these results are therefore shown. In figure 4 the streamwise momentum thickness is displayed for the upper and lower surfaces and the results compare well with the two-dimensional results. In figure 5 the pressure distributions of both VII methods are seen to be in good agreement. Close to the leading edge there are however some small differences.

6.2 Three-dimensional wing flow

To simulate fully three-dimensional wing flow, the method is applied to a 45^o swept RAE101 wing of aspect ratio 5. The grid is constructed from 71 points around the wing section, parallel to the freestream direction, and 11 points in the spanwise direction, as seen in figure 6

Pressure measurements for this wing have been done in the $11\frac{1}{2}$ ft. $\times$ $8\frac{1}{2}$ ft. wind tunnel at the R.A.E. and are reported in [25]. The tests were performed at a Reynolds number of 1.68×10^6 and at a wind speed low enough to treat the flow as incompressible.

In figures 7, 8 and 9 the measured and computed interactive and inviscid pressure distributions are shown for an incidence of 6.3^o at three different spanwise stations, $y/y_s = 0.2, y/y_s = 1.25$ and $y/ys = 1.6$. The agreement between the interactive and experimental results is good. Towards the tip however, problems were encountered with the inviscid model, due to inaccurate modelling of tip effects. No coupling therefore takes place for $y/ys > 2.2$, being the last 10% of the span, and instead the boundary layer values are determined by extrapolation.

Boundary layer velocity profiles have been measured for the same wing case by Brebner and Wyatt [2] from which the boundary layer integral thicknesses are determined [17]. The calculations are performed at an incidence of 6.3^o and a Reynolds number of 2.1×10^6. Transition is tripped close to experimentally observed locations, being $x/c = 0.08$ on the upper surface and $x/c = 0.5$ on the lower surface.

Figure 10 shows the streamwise momentum thickness computed by the three-dimensional VII program half way the wing span. The agreement with the experimental values of θ_{ss}, shown by the square points, is reasonable and similar to what Milewski achieved with his interactive method [17]. The computational methods however overpredict the boundary layer growth compared with experiment.

In figure 11 the streamwise momentum thickness at various spanwise stations is compared, showing a steeper growth near the tip of θ_{ss} at

the trailing edge.

In figures 12 and 13 the interactive and experimental shape factor H and crossflow displacement thickness δ_n^* results are shown. As said before the computed results are overpredicted but again quite similar to Milewski's results.

Figure 14 gives information about the flow of information, as one characteristic direction is nearly similar to the direction $\alpha + \beta$. It is seen that the angle between the x-axis and the limiting wall streamline is very close to 45^o, which corresponds to separation. Close to the stagnation point α is quite large, as the streamwise direction is perpendicular to the x-axis.

In figure 15 the global iteration process is plotted, in which quite a rapid error decay is seen.

The calculations have been performed on a HP unix work station and for the above flow case of three-dimensional wing flow 75 minutes of CPU time were required to converge.

6.3 Concluding remarks

Fully quasi-simultaneous coupling has been described for three-dimensional incompressible flow over wing configurations. Three interaction laws have been derived from the used Dirichlet panel method, and have been integrated in the fully three-dimensional quasi-simultaneous interaction scheme. Its capability of modelling three-dimensional flow over an unswept NACA0012 wing and 45^o swept RAE101 wing is successful. The theory is to be further tested and improved. A more accurate discretisation scheme is to be implemented to deal with the turning of the characteristics, which become parallel to the leading edge at separation. Furthermore, it is hoped to overcome the problems with tip modelling in the inviscid model.

Acknowledgements

The research was funded by the University of Groningen, NL, the University of Bristol, UK, the Engineering and Physical Research Council, UK, and the Defence Evaluation and Research Agency, Farnborough, UK.

References

[1] Ashill, P.R., Wood, R.F. and Weeks, D.J. An improved, semi-inverse version of the viscous garabedian and korn method (vgk). RAE TR 87002, 1987.

[2] Brebner, G.G. and Wyatt, L.A. Boundary layer measurements at low speed on two wings of 45^o and 55^o sweep. ARC CP 554, 1961.

[3] Brown, K.D. *Computational Analysis of Flow Speed Axial Flow Rotors*. PhD thesis, Dept. of Aerospace Eng., University of Bristol, 1997.

[4] Coenen, E.G.M. Quasi-simultaneous coupling for wing and aerofoil flow. *Proc Domain Decomp. Meth. in Sc. and Eng.*, pp 197–205, Greenwich, UK, 1999.

[5] Coenen, E.G.M., Veldman, A.E.P. and Patrianakos, G. Viscous-inviscid interaction method for wing calculations. *Proc Euro. Congr. Comp. Meth. in Appl. Sc. and Eng., ECCOMAS 2000*, Barcelona, S, 2000.

[6] Cousteix J. Three-dimensional and unsteady boundary-layer computations. *Ann. Rev. Fl. Mech.*, Vol. 18, pp 173–196, 1986.

[7] Cousteix, J. and Houdeville, R. Singularities in three-dimensional turbulent boundary-layer calculations and separation phenomena. AIAA 81-4201, 1981.

[8] Drela, M. and Giles, M.B. Viscous-inviscid analysis of transonic and low reynolds number airfoils. *AIAA J.*, Vol. 25, pp 1347–1355, 1987.

[9] Edwards, D.E. Analysis of three-dimensional flow using interacting boundary-layer theory. *Proc IUTAM Symp. on Boundary-Layer Separation*, pp 163–178, 1987.

[10] Edwards, D.E. and Carter, J.E. Analysis of three-dimensional separated flow with the boundary-layer equations. AIAA 85-1499, 1985.

[11] Green, J.E. Application of head's entrainment method to the prediction of turbulent boundary layers and wakes in compressible flow. RAE TR 72079, 1972.

[12] Houwink, R. and Veldman, A.E.P. Steady and unsteady flow computations for transonic airfoils. AIAA 84-1618, 1984.

[13] Jameson, A., Schmidt, W. and Turkel, E. Numerical solutions of the euler equations by fi-

nite volume methods using runge-kutta time-stepping schemes. AIAA 81-1259, 1981.

[14] Kerwin, J.E., Kinnas, S.A., Lee, J.-T. and Shih, W.-Z. A surface panel method for the hydrodynamic analysis of ducted propellers. *SNAME Transactions*, Vol. 95, pp 93–122, 1987.

[15] Lazareff, M. and Le Balleur, J.C. Computation of three-dimensional flows by viscous-inviscid interaction using the 'mzm' method. AGARD CP-412, 1986.

[16] Lock, R.C. and Williams, B.R. Viscous-inviscid interactions in external aerodynamic. *Progr. Aero. Sc.*, Vol. 24, pp 51–171, 1987.

[17] Milewski, W.M. *Three-Dimensional Viscous Flow Computations Using the Integral Boundary Layer Equations Simultaneously Coupled with a Low Order Panel Method*. PhD thesis, Dept. of Ocean Eng., MIT, 1997.

[18] Morino, L. and Kuo, C.-C. Subsonic potential aerodynamics for complex configurations: A general theory. *AIAA J.*, Vol. 12, No 2, 1974.

[19] Mughal, B. and Drela, M. A calculation method for the three-dimensional boundary-layer equations in integral form. AIAA 93-0786, 1993.

[20] Myring D.F. An integral prediction method for three-dimensional turbulent boundary-layers in incompressible flow. RAE TR 70147, 1970.

[21] Nishida, B. and Drela, M. Fully simultaneous coupling for three-dimensional viscous/inviscid flows. AIAA 95-1806-C, 1995.

[22] Smith, P.D. An integral method for three-dimensional compressible turbulent boundary layer. ARC R&M 3739, 1972.

[23] Van der Wees, A.J., Van Muijden, J. and Van der Vooren, J. A fast and robust viscous-inviscid interaction solver for transonic flow about wing/body configurations on the basis of full potential theory. AIAA 93-3026, 1993.

[24] Veldman, A.E.P. New, quasi-simultaneous method to calculate interacting boundary layers. *AIAA J.*, Vol. 19, pp 79–85, 1981.

[25] Weber, J. and Brebner, G.G. Low speed tests on 45^o sweptback wings. part i: Pressure measurements on wings of aspect ratio 5. RAE R Aero 2374, 1950.

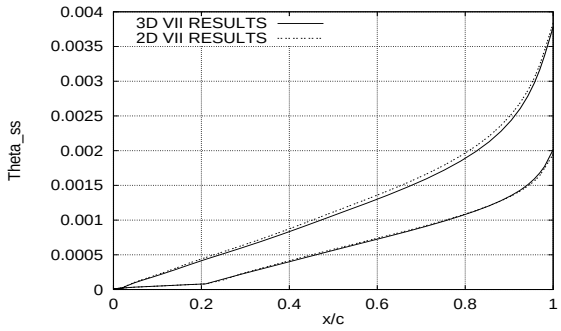

Fig. 4 Comparison of 3D and 2D interactive methods for θ_{ss}.

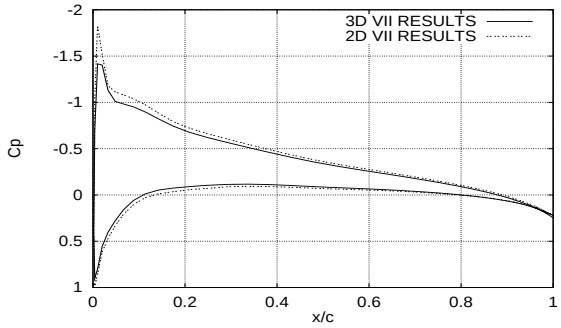

Fig. 5 Comparison of 3D and 2D interactive methods for C_p.

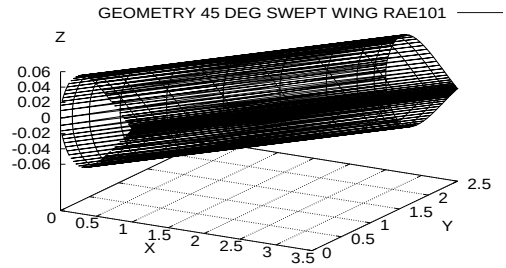

Fig. 6 Geometry RAE101 45^o swept wing.

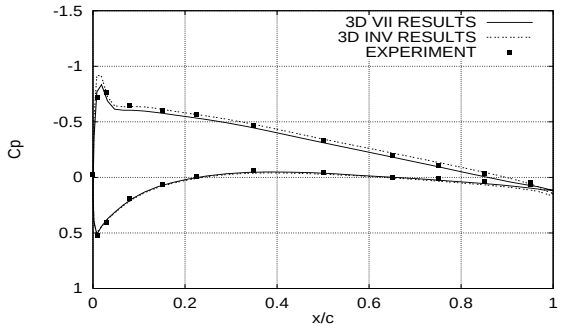

Fig. 7 Comparison inviscid, interactive and experimental C_p at $y/y_s = 0.20$.

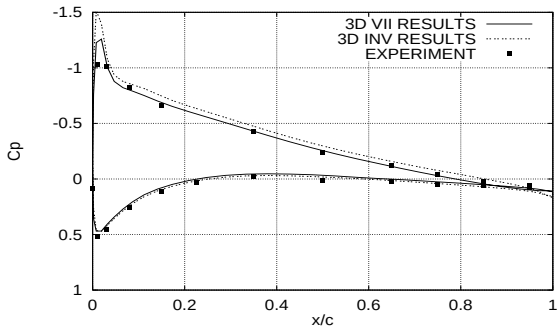

Fig. 8 Comparison inviscid, interactive and experimental C_p at $y/y_s = 1.25$.

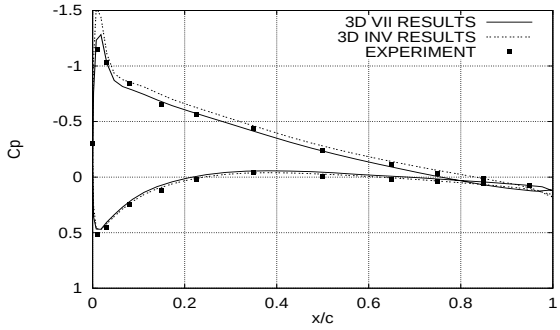

Fig. 9 Comparison inviscid, interactive and experimental C_p at $y/y_s = 1.60$.

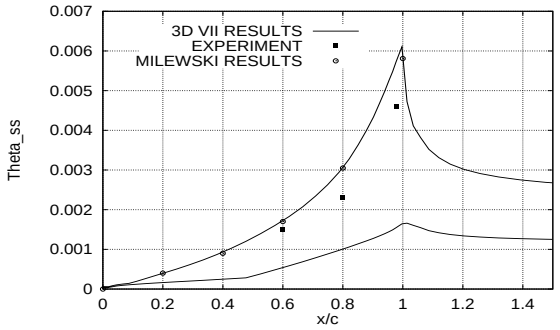

Fig. 10 Comparison interactive and experimental θ_{ss} at $y/y_s = 1.25$.

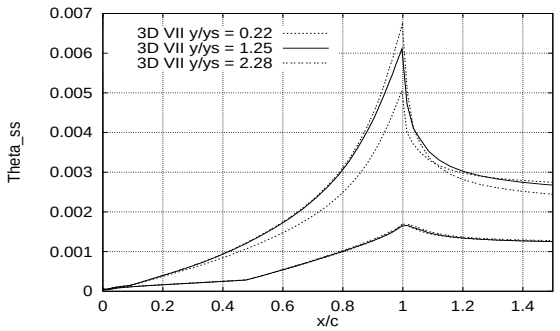

Fig. 11 Comparison θ_{ss} at different spanwise stations.

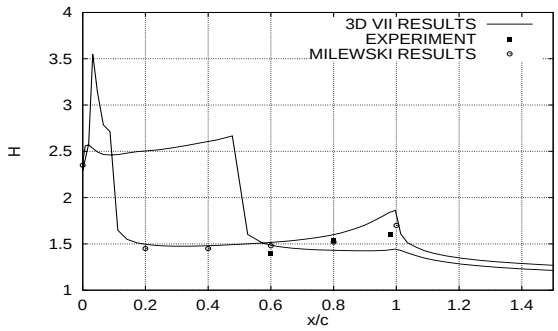

Fig. 12 Comparison interactive and experimental H at $y/y_s = 1.25$.

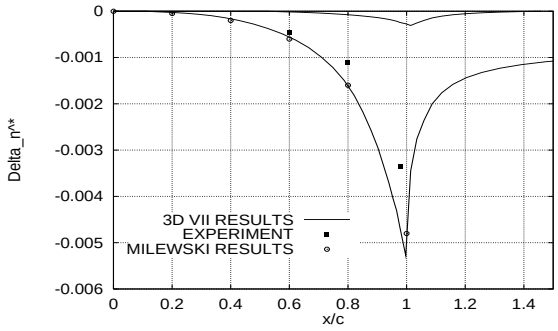

Fig. 13 Comparison interactive and experimental δ_n^* at $y/y_s = 1.25$.

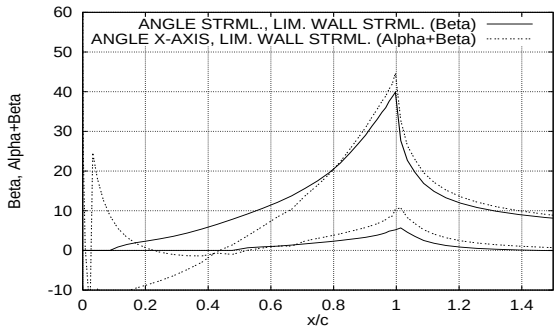

Fig. 14 Comparison β and $\alpha+\beta$ at $y/y_s = 1.25$.

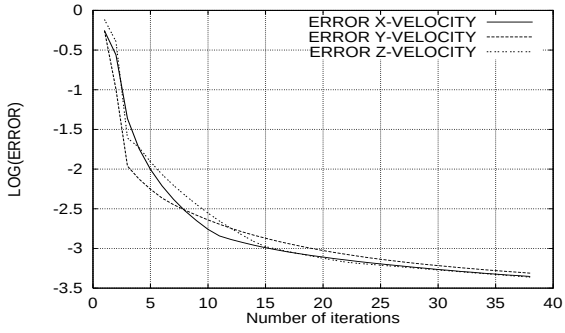

Fig. 15 Error decay versus the number of iterations.